Cerebral Cortex, August 2021;31: 3701–3712

https://doi.org/10.1093/cercor/bhab041
Advance Access Publication Date: 22 March 2021
Original Article

ORIGINAL ARTICLE

Individual Uniqueness in the Neonatal Functional Connectome

Qiushi Wang[1,2,3], Yuehua Xu[1,2,3], Tengda Zhao[1,2,3], Zhilei Xu[1,2,3], Yong He[1,2,3,4] and Xuhong Liao[5]

[1]State Key Laboratory of Cognitive Neuroscience and Learning, Beijing Normal University, Beijing 100875, China, [2]Beijing Key Laboratory of Brain Imaging and Connectomics, Beijing Normal University, Beijing 100875, China, [3]IDG/McGovern Institute for Brain Research, Beijing Normal University, Beijing 100875, China, [4]Chinese Institute for Brain Research, Beijing 102206, China and [5]School of Systems Science, Beijing Normal University, Beijing 100875, China

Address correspondence to Xuhong Liao, Ph.D. Email: liaoxuhong@bnu.edu.cn; Yong He, Ph.D. Email: yong.he@bnu.edu.cn.

Abstract

The functional connectome is highly distinctive in adults and adolescents, underlying individual differences in cognition and behavior. However, it remains unknown whether the individual uniqueness of the functional connectome is present in neonates, who are far from mature. Here, we utilized the multiband resting-state functional magnetic resonance imaging data of 40 healthy neonates from the Developing Human Connectome Project and a split-half analysis approach to characterize the uniqueness of the functional connectome in the neonatal brain. Through functional connectome-based individual identification analysis, we found that all the neonates were correctly identified, with the most discriminative regions predominantly confined to the higher-order cortices (e.g., prefrontal and parietal regions). The connectivities with the highest contributions to individual uniqueness were primarily located between different functional systems, and the short- (0–30 mm) and middle-range (30–60 mm) connectivities were more distinctive than the long-range (>60 mm) connectivities. Interestingly, we found that functional data with a scanning length longer than 3.5 min were able to capture the individual uniqueness in the functional connectome. Our results highlight that individual uniqueness is present in the functional connectome of neonates and provide insights into the brain mechanisms underlying individual differences in cognition and behavior later in life.

Key words: functional connectome, fingerprint, individual difference, neonate, resting-state fMRI

Introduction

Individual differences in the functional architecture of the human brain underlie intersubject variability in cognition, emotion, and behavior (Kelly et al. 2012; Finn and Todd 2016; Rosenberg et al. 2016). Resting-state functional magnetic resonance imaging (R-fMRI) provides a promising technique to non-invasively measure the spontaneous functional activities of the human brain *in vivo* and to map the individual functional connectivity between regions (Biswal et al. 1995; Fox and Raichle 2007). Numerous R-fMRI studies have reported remarkable individual differences in the functional connectivity profile (Mueller et al. 2013; Gao et al. 2014; Gratton et al. 2018; Xu et al. 2019; Stoecklein et al. 2020) and functional network topology (Laumann et al. 2015; Gordon et al. 2017; Liao et al. 2017) for both neonates and adults, with larger variability mainly in the association regions and lower variability in the primary regions. Specifically, several studies have suggested that in adults, the individual functional connectome is unique to serve as a fingerprint to identify individuals among a large cohort with high accuracy (Finn et al. 2015; Vanderwal

et al. 2017; Liu et al. 2018; Horien et al. 2019) and is related to individual cognitive abilities (e.g., fluid intelligence) (Finn et al. 2015). This individual distinctiveness of the functional connectome increases with age from childhood and adolescence into adulthood (Kaufmann et al. 2017), indicating a gradual maturational process of individual uniqueness. However, the extent to which an individual functional connectome is unique in the early developmental stage is unclear.

The functional network of the human brain is largely immature at birth (Cao et al. 2017b; Gilmore et al. 2018; Zhao et al. 2019). In neonates, the higher-order brain systems (e.g., default-mode and frontoparietal systems) exhibit spatially localized patterns with limited long-range connections, although the primary brain systems are well developed and exhibit a network architecture similar to that in adults (Gao et al. 2015a, 2015b; Cao et al. 2017a; Zhang et al. 2018). The default-mode network reaches an adult-like topology at the age of one year, while the frontoparietal network remains premature at the age of two years (Gao et al. 2015a, 2015b). The functional hubs are mainly located in the primary sensory and motor regions at birth (Fransson et al. 2011; Cao et al. 2017a), and shift towards the default-mode regions involved in higher-order cognitive processing during the first two years (Gao et al. 2011). In parallel to these age-related increases in functional integration, the inter-subject variability in functional networks shows an adult-like spatial pattern at birth (Xu et al. 2019; Stoecklein et al. 2020), and the magnitude of the variability substantially changes during the first two years (Gao et al. 2014). Given that the state of the functional connectivity is highly immature at birth and that the individual differences continually change with development, whether and how functional connectivity patterns in neonates are unique remains to be elucidated. Studying the individual uniqueness of the neonatal functional connectome is important for understanding the brain mechanisms underlying cognitive and behavioral differences later in life.

To address this issue, we employed a multiband R-fMRI dataset of 40 neonates obtained from the Developing Human Connectome Project (dHCP) (https://data.developingconnectome.org/) (Hughes et al. 2017) and performed a split-half network analysis to explore the individual uniqueness of the brain functional networks in neonates. Using an anatomy-constrained functional parcellation scheme of the neonatal brain (Shi et al. 2018), we constructed individual functional networks at the regional level for each neonate and identified individuals based on the functional connectivity profiles. We aimed to investigate: (1) whether functional connectivity patterns are unique in the neonatal brain, which has a highly immature functional architecture; (2) if so, which brain regions or functional systems make dominant contributions to individual uniqueness; and (3) how long the scanning length is required to capture individual uniqueness in the functional organization of the neonatal brain.

Materials and Methods

Participants and Data Acquisition

We used a publicly available dataset comprising multiband R-fMRI scans of 40 healthy neonates, obtained from the first data release (i.e., release 1) of the dHCP (https://data.developingconnectome.org/) (Hughes et al. 2017). Forty healthy neonates were born at term age (range: 36.0–41.6 weeks, mean = 39.0 weeks) and were imaged shortly after birth (interval between birth and scanning range: 0.1–3.9 weeks, mean = 0.9 weeks). The data from all neonates did not show major structural or destructive lesions and thus were included in this study. Table 1 illustrates the detailed demographic information of the participants. The neonates' parents/guardians provided informed consent, and the scanning and released protocol was approved by the UK Health Research Authority.

All MRI scans were obtained with a 3 T Philips scanner equipped with a neonatal 32 channel phased array head coil at Evelina Neonatal Imaging Center in London. Each neonate underwent multimodal MRI scanning during natural sleep over 63 min, including structural MRI, R-fMRI, and diffusion tensor imaging scanning. For each neonate, the R-fMRI scans were acquired using an accelerated echo-planar imaging sequence with the following parameters: multiband factor = 9, repetition time (TR) = 392 ms, echo time (TE) = 38 ms, 2.15 mm isotropic voxels, and 2300 volumes (i.e., 15 min). The T2-weighted structural images were acquired in sagittal and axial stacks using a turbo spin-echo sequence with the following parameters: TR = 12 s, TE = 156 ms, in-plane resolution = 0.8×0.8 mm^2, 1.6-mm slice thickness with 0.8 mm overlap, and SENSE factors of 2.11 (axial) and 2.58 (sagittal).

Data Preprocessing

We used minimally preprocessed R-fMRI images (Fitzgibbon et al. 2016), which involved susceptibility distortion correction with field maps, head motion correction with the alignment of all volumes to the volume with the lowest motion, 2-stage coregistration to the T2-weighted image, and ICA denoising with FSL FIX (Salimi-Khorshidi et al. 2014).

These images were further preprocessed using SPM12 (https://www.fil.ion.ucl.ac.uk/spm/) and GRETNA (Wang et al. 2015) (https://www.nitrc.org/projects/gretna/) as follows. First, the coregistered functional images of each neonate were spatially normalized to a neonate-specific template (Shi et al. 2011), by applying the transformation parameters estimated during the spatial normalization of the individual T2-weighted image to the template, and then, the images were resampled to 2-mm isotropic voxels. The quality of the spatial normalization was ensured by visual inspection and quantitative evaluation. Second, the functional images were split into two sections (i.e., Section 1 and Section 2) with the same scanning lengths, which were included in the subsequent individual identification analyses. Specifically, we first discarded the volumes of the first 10 s (i.e., 26 volumes) to account for image instability and then removed the volumes corresponding to 60 s (i.e., 154 volumes) in the middle of the remaining data, resulting in two separate sections (i.e., Section 1 and Section 2) with equal scanning lengths (1060 volumes). The removal of the 60-s volumes was used to reduce the influence of the temporal autocorrelation of signals between two sections. Finally, we performed linear detrending, multivariate linear regression of nuisance covariates, and temporal bandpass filtering (0.01–0.08 Hz) for Section 1 and Section 2 separately. Of note, during the nuisance regression, we regressed out 24 head motion parameters (Friston et al. 1996) and the white matter, cerebrospinal fluid, and global brain signals (Birn et al. 2006; Ciric et al. 2017) to further reduce the influence of non-neural signals. The white matter signal is supposed to capture head motion and scanner-related artifacts, while the global brain regressor is associated with motion and respiratory signals as well as hardware artifacts (e.g., head coil malfunction) (Birn et al. 2006; Power et al. 2017). To extract the tissue signals of interest,

Table 1 Demographic information of the neonates

Number of neonates	Sex (male/female)	Gestational age at birth (weeks)	Postmenstrual age at scan (weeks)
40	25/15	39.0 ± 1.7 (range: 36.0–41.6)	39.9 ± 2.1 (range: 36.9–44.1)

we employed prior neonatal-specific tissue probability maps (Shi et al. 2011), which are in a common space with the template used for spatial normalization. Here, a high threshold (i.e., 0.9) was applied to the white matter probability map to identify deep white matter voxels whose signals show weak correlations with the global brain signal (Power et al. 2017). The resulting time courses of the two sections (i.e., Section1 and Section 2) were used for the subsequent analyses.

Functional Network Construction and Reliability Analysis

We constructed individual whole-brain functional networks with GRETNA (Wang et al. 2015). For each neonate, we constructed a functional network for each section (i.e., Section 1 and Section 2) separately, wherein the nodes represented the regions of interest (ROIs) and the edges represented the internode functional connectivities. Specifically, the cortical and subcortical gray matter was parcellated into 223 nodal ROIs according to a neonate-specific functional parcellation scheme (Shi et al. 2018). The use of the functional parcellation scheme can increase the accuracy in estimating functional connectivity due to the higher functional homogeneity of voxels within each ROI than those in the structural parcellation.

We extracted the nodal time courses by averaging the voxels' time courses within each node and then estimated the internode functional connectivity by calculating the Pearson's correlation coefficient between their time courses. As a result, we obtained a 223×223 functional connectivity matrix for each section of each neonate. A group-level functional connectivity matrix was also obtained for each section, by averaging the Fisher's *r*-to-z transformed individual matrices across neonates followed by an inverted Fisher's transformation.

Next, we assessed whether the functional connectivity pattern was stable between Section 1 and Section 2. At the group level, we calculated the spatial similarity of the group-level matrices between two sections by calculating Pearson's correlation coefficient across all the lower triangular elements. At the individual level, for each neonate we estimated the intrasubject spatial similarity of the connectivity matrices between two sections. For each neonate, we also estimated the intersubject similarity between two sections as the averaged spatial similarity of this neonate in one section with all the other neonates in the other section, including the intersubject similarity from Section 1 to Section 2 and that from Section 2 to Section 1.

Individual Identification Analysis

To explore the uniqueness of the functional connectivity pattern of the neonates, we performed an individual identification approach proposed in a previous study (Finn et al. 2015). The higher the identification accuracy was, the more unique the functional connectivity pattern. The individual identification analysis involved two directions, one from Section 1 to Section 2 and the other from Section 2 to Section 1. In the first direction (i.e., from Section 1 to Section 2), we compared the functional connectivity matrix of each neonate in Section 1 with those of all the neonates in Section 2. The spatial similarity between neonates was evaluated according to the Pearson's correlation coefficient across the connectivities in the lower triangular matrix. If the neonate who showed the highest similarity in Section 2 was the same neonate given in Section 1, the identification was correct; otherwise, it was not. Finally, we calculated the accuracy rate for the neonatal population as the fraction of neonates who were identified correctly. In the second direction (i.e., from Section 2 to Section 1), Section 1 and Section 2 were reversed, and the individual identification process was repeated as described above.

Connectivity-Wise Contribution to Individual Identification

As suggested in previous studies, individual differences in functional connectivity were spatially inhomogeneous (Mueller et al. 2013; Finn et al. 2015). To ascertain which connectivities contributed the most to the individual identification process, we used two measures: group consistency (GC) and differential power (DP) (Finn et al. 2015). Connectivities showing high GC values are highly consistent across time, while those with high DP values are thought to make a large contribution to individual identification.

The estimations of GC and DP depend on the estimation of the intersection spatial similarity between two functional connectivity matrices. Specifically, the spatial similarity r_{ij} between the z-scored functional connectivity matrix of neonate *i* in Section 1 and that of neonate *j* in Section 2 can be estimated as follows:

$$r_{ij} = \frac{1}{N-1}\sum_{e} r(e)_{ij}, \quad e = 1, \ldots, N, \tag{1}$$

$$r(e)_{ij} = FC(e)_i \times FC(e)_j, \tag{2}$$

where $FC(e)_i$ and $FC(e)_j$ denote the strength of connectivity *e* in the connectivity matrices of interest after z-score transformation for neonates *i* and *j*, respectively. Since r_{ij} is estimated as the summation of $r(e)_{ij}$ across all *N* connectivities, the term $r(e)_{ij}$ can be used to denote the similarity in connectivity *e* between neonate *i* in Section 1 and neonate *j* in Section 2.

Given connectivity *e*, the GC value is calculated as

$$GC(e) = \frac{1}{N_{sub}}\sum_{i} r(e)_{ii}, \tag{3}$$

where $r(e)_{ii}$ denotes the similarity in connectivity *e* of neonate *i* between Section 1 and Section 2, and N_{sub} denotes the total number of neonates (i.e., 40 here). A high GC value means that the strength of this connectivity tends to be consistent across sections. We calculated GC for each functional connectivity and obtained a 223×223 GC matrix for the neonatal population.

Given connectivity *e* in subject *i*, if the connectivity positively contributes to the identification of the individual, it should

satisfy $r(e)_{ii} > r(e)_{ij}$ for the identification process from Section 1 to Section 2 and $r(e)_{ii} > r(e)_{ji}$ for the identification process from Section 2 to Section 1. The DP for connectivity e at the individual level is calculated as

$$DP_i(e) = -\ln \frac{\left(\left|r(e)_{ii} < r(e)_{ij}\right| + \left|r(e)_{ii} < r(e)_{ji}\right|\right)}{2\left(N_{sub} - 1\right)}, \quad (4)$$

where $|r(e)_{ii} < r(e)_{ij}|$ and $|r(e)_{ii} < r(e)_{ji}|$ denote the total number of times that $r(e)_{ii} < r(e)_{ij}$ and $r(e)_{ii} < r(e)_{ji}$ across all other neonates j, respectively. The DP for connectivity e for the neonatal population is calculated as

$$DP(e) = \sum\nolimits_i DP_i(e). \quad (5)$$

The larger the DP value is, the greater the contribution of this connectivity to individual identification. We calculated the DP value for each connectivity and thus derived a 223×223 DP matrix.

Spatial Distributions of the Connectivity-Wise GC and DP Values

To assess the potential spatial inhomogeneity in the contribution to individual identification, we assessed how the connectivity-wise GC and DP values varied across regions and across systems, and whether they were associated with inter-regional distances.

Regional level. We estimated the GC and DP values for each node by averaging the GC and DP values, respectively, across all the connectivities of this node. The ROIs with high GC values represented ROIs that were highly consistent across two sections, while the ROIs with high DP values represented ROIs that made large contributions to individual uniqueness.

System level. We identified the functional systems of the neonates by using a modular detection approach. Specifically, for both sections (i.e., Section 1 and Section 2), we generated a group-level weighted functional network by thresholding the group-level functional connectivity matrix with a network density of 10%, wherein connectivities with negative connectivities were excluded due to their ambiguous interpretations (Weissenbacher et al. 2009; Murphy and Fox 2017). Next, we detected the modular architecture in the group-level functional network for each section using the Infomap algorithm (Rosvall and Bergstrom 2008), which captures the structured pattern of information flow on the network and has been used to identify brain modules in agreement with the task-driven functional systems (Power et al. 2011). Given the modular partition of the network, an index of modularity was estimated to quantify the strength of the modular division (Newman and Girvan 2004). The spatial similarity of the modular architectures between Section 1 and Section 2 was assessed using adjusted mutual information (AMI) (Vinh et al. 2010). As the modular architectures were highly similar between the two sections, the modular architecture derived from Section 1 was used as the reference for the functional systems of the neonates.

The within-system contribution to individual identification was quantified by averaging the connectivity-wise GC (or DP) values within each module, and the between-system contribution was quantified by averaging the GC (or DP) values across the between-module connectivities. We quantified the overall contribution of each module by averaging the GC (or DP) values across all the connectivities involved with each module.

Spatial distance influence. To explore the spatial distance dependence of connectivity-wise GC and DP values, we calculated the Euclidean distance between each pair of nodes and divided all connectivities into three groups with different ranges of Euclidean distances, including the short-range of 0–30 mm, the middle range of 30–60 mm and the long range of 60–120 mm. The Euclidean distances among regions were estimated in the standard space (i.e., the neonate-specific template), in order to correct for intersubject variability in brain sizes and make the cross-individual comparison feasible. We then compared the GC and DP values of the connectivities across different distance ranges. To correct for the multiple comparisons, the Bonferroni method was used with a corrected $P < 0.05$.

Effects of Scanning Lengths on Individual Identification

To determine the appropriate scanning length for identifying individuals from the functional connectivity pattern in neonates, we performed the following analysis. In brief, for each section in each neonate, we obtained various R-fMRI segments with increasing scanning lengths from 30 to 390 s in steps of 30 s. To ensure that the scanning interval between two sections was the same (i.e., 60 s), the segments in Section 1 were obtained by truncating volumes from the end to the beginning, and the segments in Section 2 were obtained by truncating volumes from the beginning to the end. For a given scanning length, we constructed individual functional connectivity matrices for each section and performed the individual identification process as described before. The dependence of individual identification accuracy on the scanning length was investigated.

Validation Analysis

We evaluated whether our main results were influenced by different data preprocessing and analysis strategies, including head movement correction, global signal regression, and removal of weak connectivities, as well as age and sex effects.

Head movement correction. Head movement during data acquisition could bias the estimation of functional connectivity (Power et al. 2012; Satterthwaite et al. 2012; Van Dijk et al. 2012). To mitigate the influence of head motion, we included the 24 head motion parameters (Friston et al. 1996) and the global brain signal (Yan et al. 2013; Ciric et al. 2017) in the nuisance regression during the data preprocessing. To explore the potential residual influence of head motion, we further performed a data scrubbing on the preprocessed functional images (Power et al. 2012, 2013; Power et al. 2015). For each section of each neonate, we calculated the framewise displacement (FD) (Power et al. 2012) for each time point and discarded the "bad" volumes with FD above 0.2 mm and their adjacent volumes (i.e., 1 backward and 2 forward). Neonates who had "bad" volumes in more than 50% of the original data in either of the two sections were excluded. Finally, we estimated the individual functional connectivity matrices based on the remaining data and repeated the individual identification analysis.

Global signal regression. Global signal regression is a controversial issue in R-fMRI data analysis, which affects the distribution of functional correlations as well as the network topology (Murphy and Fox 2017). In the main analysis, we preprocessed the R-fMRI data with the global signal included in the nuisance

regression, to better reduce the influence of physiological noise and head motion (Birn et al. 2006; Yan et al. 2013; Power et al. 2017). To assess the potential influence of the global signal, we reperformed all the analyses based on functional data without global signal regression during data preprocessing.

Removal of weak connectivities. In the main analysis, all functional connectivities were included in the individual identification. However, in the functional networks, some weak connectivities might be spuriously induced by noise. To assess the potential influence of spurious connectivities, we identified strong connectivities for each section using the following procedures. Given a section (i.e., Section 1 or Section 2), we performed a one-sample t-test across all the neonates for every connectivity and identified the strong connections as those surviving from the correction for multiple comparisons ($q < 0.05$, FDR corrected). Then, we repeated the individual identification analysis based on the strong connectivities in common for both sections.

Age and sex effects. Age and sex are two important factors affecting brain connectivity patterns (Gong et al. 2011; Gao et al. 2017; Gilmore et al. 2018). Due to individual differences in age and sex among the neonates (see Table 1), our results may be affected by these two factors. Here, we explored the potential influence of age and sex on the connectivity-wise contribution to individual identification (i.e., DP). For each connectivity, we employed a general linear model, which included age, sex, and their interaction as predictors:

$$Y_i = \beta_0 + \beta_1 \times age_i + \beta_2 \times sex_i + \beta_3 \times (age_i \times sex_i) + \beta_4 \times mFD_i + \varepsilon_i, i = 1, 2, \ldots, N_{sub}, \quad (6)$$

where Y_i represents the DP value of the connectivity of interest for neonate i. The head motion parameter mFD_i, which denotes the averaged FD across two sections, was also included as a covariate. The significant effect of each predictor was corrected for multiple comparisons across connectivities ($q < 0.05$, FDR corrected). For the connectivities showing significant interaction effects, the age effects were evaluated in girls and boys separately. Of note, in the general linear model, postmenstrual age at scan and chronological age at scan were separately considered to take into account different types of developmental influence.

Results

Individual Identification in Neonates Based on Whole-Brain Functional Connectivity Patterns

We used a neonate-specific functional parcellation scheme to construct the individual functional connectivity matrices (Fig. 1A). Group-level connectivity matrices for Section 1 and Section 2 are displayed in Fig. 1B. The group-level connectivity matrices showed high spatial similarity between Section 1 and Section 2 ($r = 0.94$, $P < 0.0001$) (Fig. 1B), indicating reliable functional connectivity patterns at the group level. At the individual level, we also observed high spatial similarities within the same neonates (rs, mean ± std = 0.54 ± 0.09), which were significantly higher than those estimated between different neonates either from Section 1 to Section 2 (rs, mean ± std = 0.19 ± 0.05) or the reverse direction (rs, mean ± std = 0.19 ± 0.05) (both $ps < 0.0001$, paired t-tests) (Fig. 1C). Based on the whole-brain functional connectivity patterns, the neonates were successfully identified between the two sections with an accuracy of 100% in both directions (Fig. 1D), suggesting that the individual uniqueness was present in the functional connectivity profiles of the neonates.

Spatial Distribution of the Connectivities with High GC and DP Values

We estimated the GC and DP values for each connectivity and summarized them at the regional and system levels. First, we found that regions with high GC values were primarily located bilaterally in the superior frontal gyrus, parietal cortex and sensorimotor areas (Fig. 2A, left). Regions with high DP values were mainly located in the medial and lateral frontal cortices, superior parietal gyrus, anterior and middle cingulate gyri, and left inferior temporal gyrus (Fig. 2A, right). Next, we assessed whether the distributions of the GC and DP values were dependent on the functional system. For the group-level functional network of Section 1, the network modularity was 0.58, and eight modules were detected (Fig. 2B), including sensorimotor/auditory, prefrontal, orbitofrontal, subcortical, visual, parietal/temporal, left temporal, and right temporal modules. This modular architecture was highly similar to that obtained from Section 2 (Fig. S1) (AMI = 0.80) and was hereafter used as the reference for the functional systems. We found that the connectivities with the highest GC values (i.e., top 0.5%) were primarily located within several systems, including the prefrontal, sensorimotor/auditory, parietal/temporal, and visual systems (Fig. 2C, left), and those with the highest DP values (i.e., top 0.5%) were primarily located between systems (Fig. 2D, left). Similar results were observed for different thresholds of the highest values (i.e., top 3%, 5%, and 10%) (Fig. S2). At the system level, the prefrontal, sensorimotor/auditory, parietal/temporal, and visual modules showed the largest GC values (Fig. 2C, right), and the prefrontal and parietal/temporal modules showed the largest DP values (Fig. 2D, right).

We also examined the distance dependence of the connectivity-wise GC and DP values. All connectivities were classified into three groups with inter-region Euclidean distances located within different bins, including 0–30, 30–60, and 60–120 mm. We found that the short-range connectivities (0–30 mm) showed significantly higher GC values than the connectivities at the other distance ranges (30–60 and 60–120 mm) (all $ps < 0.0001$, two-sample t-tests), and the middle-range connectivities (30–60 mm) showed significantly higher GC values than the long-range connectivities (60–120 mm) ($P < 0.0001$, two-sample t-test). Meanwhile, the short- and middle-range connectivities (0–30 and 30–60 mm) showed significantly higher DP values than the long-range connectivities (60–120 mm) (both $ps < 0.0001$, two-sample t-tests) (Fig. 3). These results suggest that short- and middle-range connectivities may dominantly contribute to the identification of neonates.

Effects of Scanning Lengths on Individual Identification

We divided each scanning section (i.e., Section 1 and Section 2) into thirteen bins with increasing scanning lengths ranging from 0.5 to 6.5 min in steps of 0.5 min (Fig. 4A). With a scanning length of 0.5 min, the accuracy of individual identification was relatively low in both directions (55% for Section 1 to Section 2 and 62.5% for Section 2 to Section 1) (Fig. 4B). As the scanning length increased, the identification accuracies in both directions increased gradually and finally reached a saturation point.

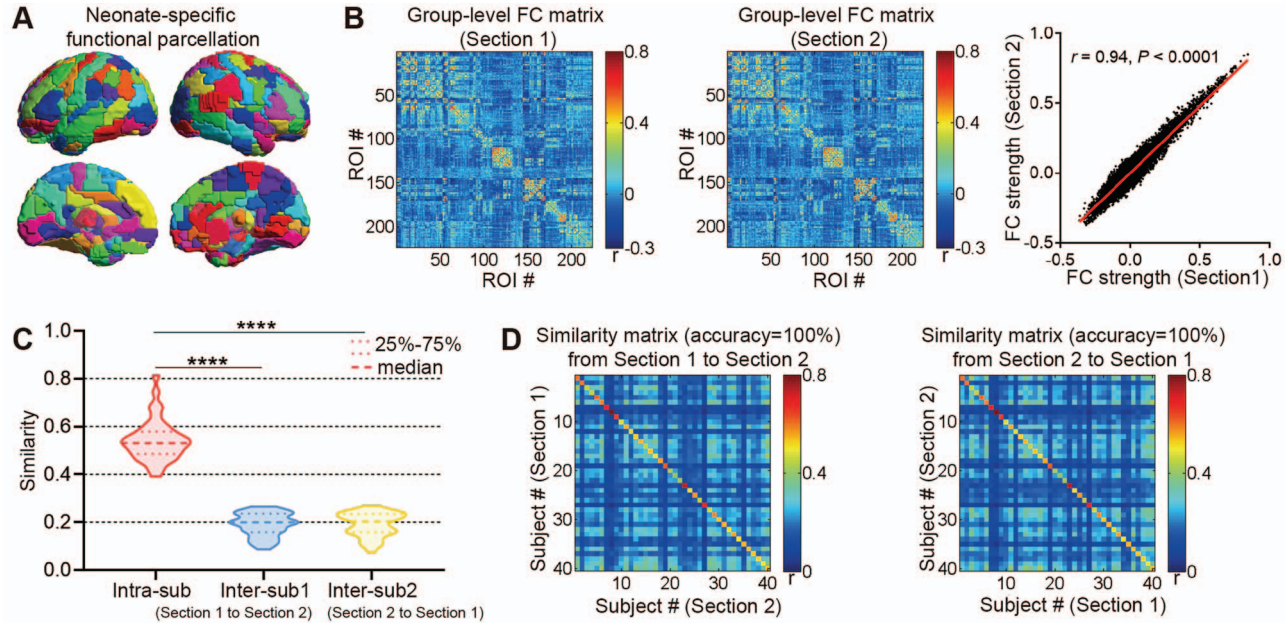

Figure 1. Individual identification in neonates using whole-brain FC patterns. (*A*) Neonate-specific functional parcellation with 223 nodes. (*B*) Group-level functional connectivity matrices for Section 1 (left) and Section 2 (middle), and significant spatial correlation in the whole-brain connectivity patterns between two sections (right). Each dot in the scatter plot represents a connectivity in the group-level matrices. (*C*) Spatial similarity of individual FC patterns between two sections. For each neonate, we calculated the spatial similarity within the same subjects (intra-sub, red), the mean spatial similarity of this subject in Section 1 with all the other subjects in Section 2 (inter-sub, Section 1 to Section 2, blue), and the mean spatial similarity of this subject in Section 2 with all the other subjects in Section 1 (inter-sub, Section 2 to Section 1, yellow). (*D*) Intersubject similarity matrices of FC patterns from Section 1 to Section 2 (left) and from Section 2 to Section 1 (right). Each row represents the spatial similarities (i.e., Pearson's correlation coefficients) between one neonate in Section 1 (Section 2) and all neonates in Section 2 (Section 1). ****, Bonferroni corrected $P < 0.0001$. FC: functional connectivity. ROI: region of interest.

Notably, the identification accuracy was as high as 100% with a scanning length of 3.5 min, regardless of the identification direction. This finding suggests that a scanning length of at least 3.5 min leads to successful neonate identification.

Effects of Head Movement on Individual Identification

For the 40 neonates included in the main analysis, the mean FD across time for each neonate ranged from 0.10 to 0.90 mm (mean ± std = 0.27 ± 0.18 mm) for Section 1 and from 0.10 to 1.17 mm (mean ± std = 0.31 ± 0.24) for Section 2. To reduce the effects of transient head motion, we discarded the volumes with large head movement. Thirteen neonates remained after data scrubbing with a stringent criterion (proportion of volumes remaining, mean ± std = 71.7% ± 10.7% for Section 1 and 71.1% ± 15.0% for Section 2). For the remaining neonates, the accuracy of individual identification was 100% in both directions. The spatial distributions of the GC and DP values at the regional and system levels remained nearly unchanged (Fig. 5). These results suggest that head movement had little influence on our main findings.

Effects of Other Factors

We validated our results by using different data preprocessing and analysis strategies, including global signal regression, removal of weak connectivities, and consideration of age and sex effects. (1) *Global signal influence*. After preprocessing the R-fMRI data without global signal regression, we found that the individual identification accuracy was 100% in both directions, and the spatial distributions of the GC and DP values were highly similar to our main results (Fig. S3). These results indicate a weak influence of the global signal on our findings. (2) *Removal of weak connectivities*. A total of 5018 strong connectivities were detected in common for both sections. Based on these strong connectivities, we repeated the individual identification analysis, and the main results showed few changes (Fig. S4). Of note, the accuracy was 100% for individual identification from Section 1 to Section 2 and 97.5% for identification from Section 2 to Section 1. These results suggest that our main findings were not driven by weak connectivities. (3) *Effects of age and sex on the DP value*. Two types of ages (i.e., postmenstrual and chronological ages at scan) were separately included in the general linear model. For postmenstrual age, we did not observe any significant effects of age, sex, or their interaction for any connectivity ($q > 0.05$, FDR corrected). For chronological age, we did not observe significant sex effects but found significant effects of age and age by sex interaction for some connectivities ($q < 0.05$, FDR corrected) (Fig. S5). Specifically, the DP values of a few connectivities significantly increased with chronological age, which were mainly intersystem connections involved with sensorimotor/auditory, prefrontal, and temporal systems (Fig. S5A). The connectivities showing significant interaction effects were primarily intersystem connections involved with sensorimotor/auditory, prefrontal, and orbitofrontal systems (Fig. S5B), all of which showed significant age-related increases in girls (all $ps < 0.05$). For the boys, only a few connectivities exhibited significant age effects.

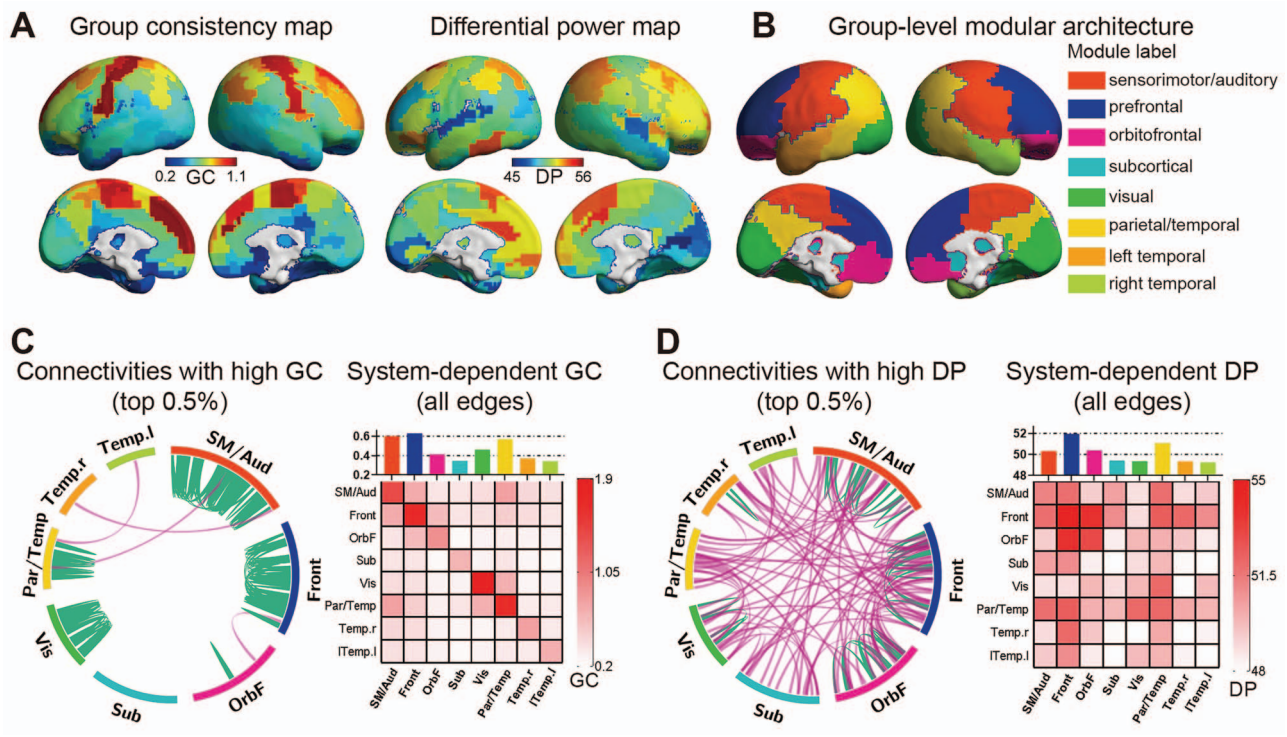

Figure 2. Spatial distributions of connectivities with high GC and DP values. (*A*) Maps of regional GC and DP values. (*B*) Modular architecture at the group level for Section 1. Eight modules were detected. (*C*) Spatial distribution of connectivity-wise GC values. Left, spatial distribution of connectivities with the top 0.5% GC values; right, GC values at the system level for all connectivities. (*D*) Spatial distributions of connectivity-wise DP values. Left, spatial distribution of connectivities with the top 0.5% DP values; right, DP values at the system level for all connectivities. In (*C*) and (*D*), each element in the matrices denotes the average GC or DP values within each module or between each pair of modules. The value of each bar above the matrices represents the average GC or DP value of all connectivities involved with each module. In the circle graphs, magenta and green lines represent inter- and intra-module connectivities, respectively. The BrainNet Viewer package (Xia et al. 2013) was used to display the brain surface, and Circos (Krzywinski et al. 2009) was used to display the circular distribution of GC and DP connectivities. GC, group consistency; DP, differential power; SM/Aud, sensorimotor/auditory; Front, prefrontal; OrbF, orbitofrontal; Sub, subcortical; Vis, visual; Par/Temp, parietal/temporal; Temp.r, right temporal; Temp.l, left temporal.

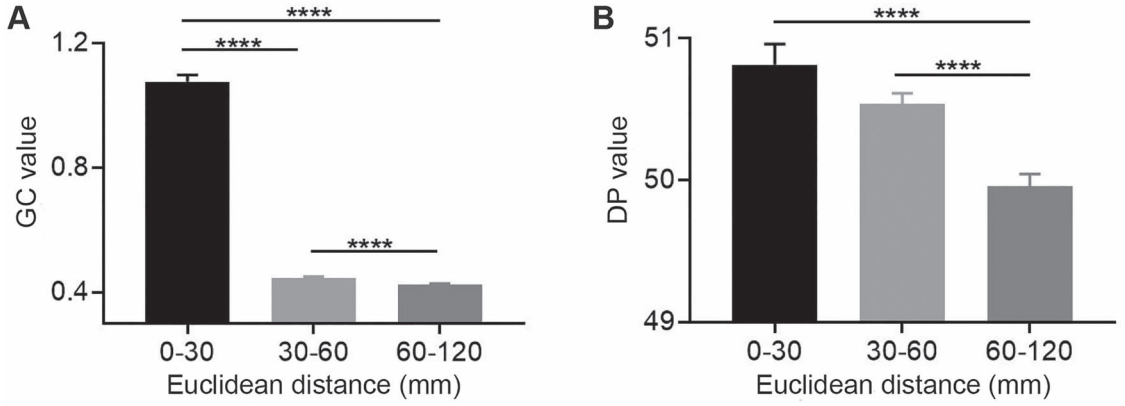

Figure 3. GC and DP values of connectivities at different distances. Each bar represents the mean GC (left) or DP (right) value of all the connectivities within each distance range, and each whisker represents the standard error of the mean. ****, Bonferroni corrected $P < 0.0001$; GC, group consistency; DP, differential power.

Discussion

Based on the multiband R-fMRI data of 40 healthy neonates, using a connectome-based individual identification approach, we demonstrated that the functional connectivity patterns of neonates are individually unique. The main findings are as follows: (1) the individual functional connectomes were reliable between the two sections, based on which all the neonates were correctly identified from the population; (2) regions in the higher-order cortices, especially in the prefrontal and parietal–temporal systems, dominantly contributed to the individual identification process; (3) the short- (0–30 mm) and middle-range (30–60 mm) connectivities showed higher DP values than the long-range (60–120 mm) connectivities; and (4) R-fMRI data with scanning lengths longer than 3.5 min were able to capture individual uniqueness in the neonatal functional connectome.

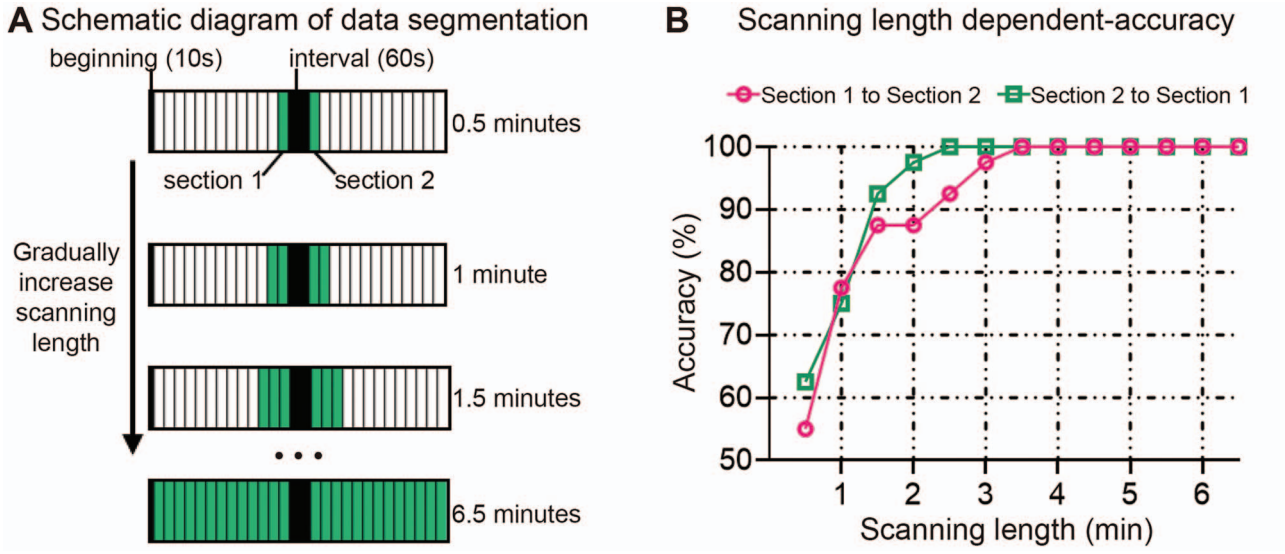

Figure 4. Scanning length effects on individual identification. (*A*) Schematic diagram of data segmentation with different scanning lengths. The total length of the bar represents the entire scanning time (15 min in total) for each neonate. We removed the R-fMRI volumes in the first 10 s and the middle 60 s (black-filled areas). Green bins refer to different data segments used for individual identification with increasing scanning lengths in steps of 30 s. (*B*) Individual identification accuracies at different scanning lengths. Magenta dots represent the identification accuracies from Section 1 to Section 2, and green dots represent the identification accuracies from Section 2 to Section 1.

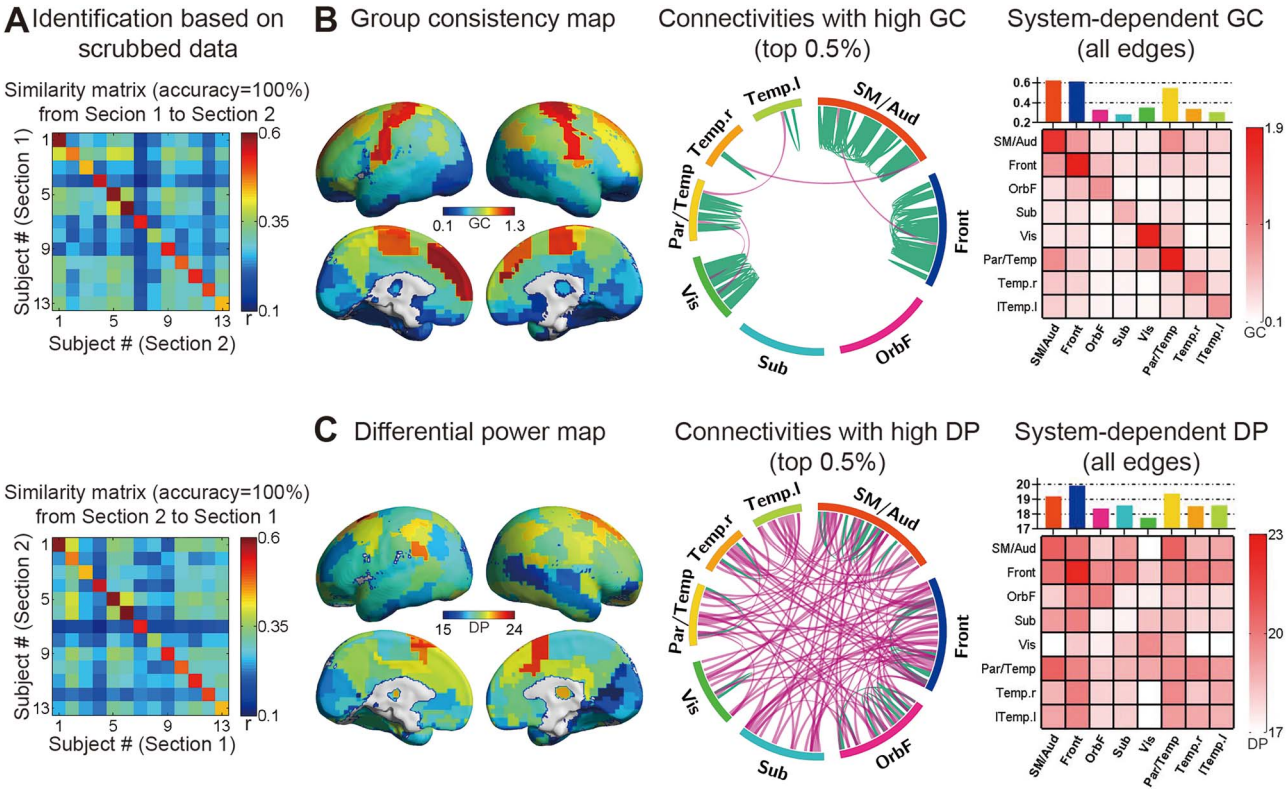

Figure 5. Head movement effects on individual identification. (*A*) Individual identification using whole-brain FC patterns estimated from scrubbed data. Individual identification was performed among the thirteen subjects who remained after data scrubbing with a stringent criterion. (*B*) Spatial distribution of GC values. Left: map of regional GC values; middle, spatial distribution of connectivities with the highest (top 0.5%) GC values; right, GC values at the system level for all connectivities. (*C*) Spatial distribution of DP values. Left, map of regional DP values; middle, spatial distribution of connectivities with the highest (top 0.5%) DP values; right, DP values at the system level for all connectivities. GC, group consistency; DP, differential power.

Our results were reproducible under the strict control of head motion and the removal of weak connectivities. These findings indicate that the individual uniqueness of the functional connectome is already present in neonates, which may shape individual differences in cognition and behavior in later developmental stages.

Individual Functional Connectomes are Unique in Neonates

Prior studies have demonstrated that the functional connectomes of adults and adolescents are individually unique (Finn et al. 2015; Vanderwal et al. 2017; Horien et al. 2019). As an expansion of previous studies, we found that the individual uniqueness of functional connectomes is already present in neonates, as evidenced by accurate individual identification between two sections. This finding is different from a recent study (Kaufmann et al. 2017) that showed that functional connectome distinctiveness matures gradually with age from childhood to adolescence into adulthood. The inconsistency may be attributed to the fact that different types of fMRI data were used in these two studies. In the study by Kaufmann et al. (2017), individual identification was performed across resting and task states. Since functional connectivity patterns are state-dependent, the cross-state comparison might reduce the accuracy, as shown in adults (Finn et al. 2015). In our study, we focused on the intrinsic functional connectome, which was acquired during natural sleep. The functional organization is relatively stable across sleep stages during the fMRI scans lasting minutes (Gao et al. 2017), which could increase the intersection similarity and improve the accuracy. The presence of uniqueness in the functional connectome at birth, a stage that is far from mature, suggests that genes and the maternal environment play a critical role in individual functional connectome development. The early established individual uniqueness in the functional connectome may not only contribute to distinctive cognition and behaviors in neonates but also lay a foundation for individual cognitive development.

Higher-Order Cortices Dominate Individual Uniqueness

In neonates, the brain regions show a differentiated maturation pattern in both functional connectivity organization (Gao et al. 2015a, 2015b) and cortical tissue characteristics (Stoecklein et al. 2020). One might expect that the more mature primary areas may better capture individual characteristics than the association areas with prolonged maturation. Nevertheless, we observed that in neonates, the regions that made dominant contributions to functional connectome uniqueness were mainly located in the higher-order brain systems, especially the prefrontal lobe, cingulate gyrus, and parietal lobe. This observation seems to be reasonable, because high intersubject variability has been observed in the functional connectivity profiles of these regions for neonates (Gao et al. 2014; Xu et al. 2019; Stoecklein et al. 2020). The positive correlation between the distinctiveness (i.e., DP value) and the intersubject variability was confirmed at both the connectivity and regional levels (Fig. S6). Although higher-order cognitive functions are far from mature at birth, functional connectivities underlying these cognitive processes may develop early and establish a neuronal basis during the prenatal stage (Thomason et al. 2015). Combined with previous findings in adults and adolescents (Finn et al. 2015; Horien et al. 2019), we suggest that the connectivity patterns of the higher-order cortices consistently capture individual characteristics at different ages. Given the remarkable reconfiguration of the connectivities of the higher-order regions in postnatal development (Collin and van den Heuvel 2013; Vértes and Bullmore 2015), their development may follow individualized trajectories to preserve a high intersubject variability from the neonatal to the adult stage (Mueller et al. 2013; Gao et al. 2014).

Of note, regional individual distinctiveness and temporal consistency are not directly related. The regions showing high differential power across individuals partially overlapped with those showing high temporal consistency, mainly in the medial prefrontal and bilateral parietal cortices. For these overlapping regions, the functional connectivities are individually distinctive and stable across repeated measurements. However, some other regions showed high DP values (e.g., inferior frontal cortex) but low GC values. This could be because the intersubject variability in their connections is large enough to differentiate individuals from each other despite the presence of intrasubject fluctuations. In contrast, some regions showed high temporal consistency but relatively low uniqueness, such as the sensorimotor areas, and this finding can be explained by the low interindividual variability in connectivity (Gao et al. 2014; Xu et al. 2019; Stoecklein et al. 2020). Similar findings were also observed at the connectivity level. The connectivities with high DP values were mainly located between different systems, while the connectivities with high GC values were predominantly located within the same systems. Moreover, we found that compared with the GC value, the DP value showed a higher spatial correspondence with the intersubject variability in functional connectivity strength at both the regional and connectivity levels (Fig. S6). On the basis of these results, we speculate that for repeated sections with short time intervals, the differential power of the brain regions may be predominantly determined by the extent of the intersubject variability rather than the temporal consistency.

We further observed that the differential power of some connectivities significantly increased with chronological age, especially for girls (Fig. S5). These connectivities were dominantly intersystem connectivities involved with sensorimotor/auditory and frontal regions, which might be related to the individualized refinements of the sensorimotor and auditory functions during postnatal development. The faster developmental rates in girls are compatible with a previous finding demonstrating the faster development of the functional network topology from birth to adolescence in girls (Gozdas et al. 2019). Our results suggest an increased distinctiveness in the connectivities during postnatal development, which is sex dependent. However, the mechanisms underlying the contributions of genetic and environmental factors to these changes remain to be deciphered. Of note, the present study employed neonates spanning a narrow range of chronological ages (i.e., 0.1–3.9 weeks). A larger sample of infants across a wider age range (e.g., including prenatal and postnatal stages) is needed to better delineate the age and sex effects in the future.

Short- and Middle-Range Connectivities are Highly Distinctive

We found that the short- and middle-range connectivities were more distinctive than the long-range connectivities, suggesting that these connectivities make a dominant contribution to individual uniqueness. In the prenatal and preterm developmental stages, the changes in functional connectivity are mainly

limited to short- and middle-range connectivities in order to enhance functional segregation (Ouyang et al. 2017), such as the enhancement of short-range connectivities during the second trimester (Jakab et al. 2014) and the strengthening of short- and middle-range connectivities during the third trimester (Cao et al. 2017a). The relatively early developments of the short- and middle-range connectivities before birth may be largely influenced by genetic and maternal factors and thus reflect individual characteristics in functional architecture, resulting in relatively high distinctiveness. In contrast, long-range functional connectivities are much less developed before birth (Smyser et al. 2010; Thomason et al. 2015; Cao et al. 2017a), likely due to the limited myelination in white matter (Collin and van den Heuvel 2013), and exhibit a prolonged maturation process from the infant stage to adulthood (Fair et al. 2009; Gao et al. 2011). A prior study pointed out that during the third trimester, the functional networks of infants transit from a relatively random architecture towards a more organized configuration (Cao et al. 2017a). Therefore, late-maturing long-range connectivities may retain a relatively random configuration in neonates and may thus be less distinguishable across individuals.

Effect of Scanning Length on Individual Identification

R-fMRI data with a sufficient scanning length are necessary to reliably map functional connectomes and infer convincing conclusions. Here, we observed that the connectome-based identification accuracy increased with scanning length, which is in line with the results of prior studies on individual identification in adults (Finn et al. 2015; Horien et al. 2018). These findings may be because a longer scanning duration increases the reliability of the functional network by increasing the degree of freedom for connectivity estimation and reducing the sampling error (Laumann et al. 2015). Of note, we found that the identification accuracy reached a plateau (i.e., 100%) after 3.5 min, which is much shorter than the scan duration (e.g., at least 5 min) needed to estimate reliable functional correlations in adults (Van Dijk et al. 2010; Whitlow et al. 2011). This result is possible and reasonable since the algorithm used for individual identification is dependent on the difference between the intrasubject similarity and the maximal intersubject correlation rather than the absolute magnitude of the intrasubject reliability (Noble et al. 2017). With a scanning length of 3.5 min, the overall connectivity pattern in neonates may yield a higher intrasubject than intersubject similarity, thus allowing individual characteristics in the functional organization to be captured. In addition, in comparison with the resting state usually adopted for adults, the relatively stable functional architectures of neonates during natural sleep (Gao et al. 2017) may also contribute by promoting intrasubject similarity between two sections. This finding indicates that individual-specific functional connectivity patterns can be captured with a short scanning duration and may provide some guidelines for future studies regarding individual differences in neonates.

Technical Considerations and Future Directions

Several issues need to be considered. First, we used a split-half approach to obtain repeated R-fMRI measurements required for individual identification, with only a short time interval (i.e., 1 min) between the two sections. The short interval may have enhanced the intrasubject reliability, as suggested in a study by Birn et al. (2013), and thus made individual identification easier than it would have been with an intersession design. Future studies should be conducted to explore individual identification with longer interscan intervals (such as hours or days) if R-fMRI data of neonates satisfying these conditions are available. Considering the rapid development of functional connectivities in infants (Cao et al. 2017b; Gilmore et al. 2018), the remarkable developmental effect may become a confounding factor for individual identification if the interscan interval extends to months or years. Second, the impact of the parcellation scheme should be investigated further. Here, to define the regions of interest, we used a neonate-specific functional parcellation scheme (Shi et al. 2018), which is anatomically constrained according to a spatially deformed automated anatomical labeling atlas of an adult (Tzourio-Mazoyer et al. 2002). Given the remarkable changes in the brain from the neonatal stage to adulthood, the anatomical boundaries in adults may not be suitable for neonatal brains and thus may affect our functional connectivity estimation. It is suggested that a neonate-specific functional parcellation scheme be constructed through a functional data-driven approach. Third, the neonatal R-fMRI data in the dHCP were obtained during natural sleep rather than the typical resting state for adults. Given potential differences in the functional architecture between the sleep and wake states (Graham et al. 2015; Mitra et al. 2017), the applicability of our findings to the resting state of neonates deserves further exploration. Finally, we found that individual uniqueness is present in the functional connectome of neonates born at term. Whether uniqueness can be observed at an earlier developmental stage (i.e., prenatal or preterm period) is still unclear. Moreover, to elucidate the functional significance of the subject-specific connectivity patterns, their potential behavioral associations are worth examining.

Notes

We thank Zilong Zeng for valuable suggestions. Data were provided by the developing Human Connectome Project, KCL-Imperial-Oxford Consortium funded by the European Research Council under the European Union Seventh Framework Programme (FP/2007-2013) / ERC Grant Agreement no. [319456]. We are grateful to the families who generously supported this trial. Some data and codes from this study are available at https://github.com/helab207/Individual-Uniqueness-of-Neonatal-FC.

Conflict of Interest. The authors have no conflicts of interest to declare.

Funding

The National Natural Science Foundation of China (nos. 31830034, 82021004, 81971690, 11835003, 81801783); Changjiang Scholar Professorship Award (T2015027); Fundamental Research Funds for the Central Universities (2019NTST24).

References

Birn RM, Diamond JB, Smith MA, Bandettini PA. 2006. Separating respiratory-variation-related fluctuations from neuronal-activity-related fluctuations in fMRI. *Neuroimage*. 31:1536–1548.

Birn RM, Molloy EK, Patriat R, Parker T, Meier TB, Kirk GR, Nair VA, Meyerand ME, Prabhakaran V. 2013. The effect of scan length on the reliability of resting-state fMRI connectivity estimates. *Neuroimage*. 83:550–558.

Biswal B, Yetkin FZ, Haughton VM, Hyde JS. 1995. Functional connectivity in the motor cortex of resting human brain using echo-planar MRI. *Magn Reson Med*. 34:537–541.

Cao M, He Y, Dai Z, Liao X, Jeon T, Ouyang M, Chalak L, Bi Y, Rollins N, Dong Q, et al. 2017a. Early development of functional network segregation revealed by connectomic analysis of the preterm human brain. *Cereb Cortex*. 27:1949–1963.

Cao M, Huang H, He Y. 2017b. Developmental connectomics from infancy through early childhood. *Trends Neurosci*. 40:494–506.

Ciric R, Wolf DH, Power JD, Roalf DR, Baum GL, Ruparel K, Shinohara RT, Elliott MA, Eickhoff SB, Davatzikos C, et al. 2017. Benchmarking of participant-level confound regression strategies for the control of motion artifact in studies of functional connectivity. *Neuroimage*. 154:174–187.

Collin G, van den Heuvel MP. 2013. The ontogeny of the human connectome: development and dynamic changes of brain connectivity across the life span. *Neuroscientist*. 19:616–628.

Fair DA, Cohen AL, Power JD, Dosenbach NU, Church JA, Miezin FM, Schlaggar BL, Petersen SE. 2009. Functional brain networks develop from a "local to distributed" organization. *PLoS Comput Biol*. 5:e1000381.

Finn ES, Shen X, Scheinost D, Rosenberg MD, Huang J, Chun MM, Papademetris X, Constable RT. 2015. Functional connectome fingerprinting: identifying individuals using patterns of brain connectivity. *Nat Neurosci*. 18:1664–1671.

Finn ES, Todd Constable R. 2016. Individual variation in functional brain connectivity: implications for personalized approaches to psychiatric disease. *Dialogues Clin Neurosci*. 18:277–287.

Fitzgibbon SP, Jenkinson M, Robinson E, Bozek J, Griffanti L, Makropoulos A, Wright R, Schuh A, Hughes E, Abei M, *et al*. 2016. The developing Human Connectome Project (dHCP): minimal functional pre-processing pipeline for neonates. In. *The Fifth Biennial Conference on Resting State and Brain Connectivity; Vienna (Austria, EU)*.

Fox MD, Raichle ME. 2007. Spontaneous fluctuations in brain activity observed with functional magnetic resonance imaging. *Nat Rev Neurosci*. 8:700–711.

Fransson P, Aden U, Blennow M, Lagercrantz H. 2011. The functional architecture of the infant brain as revealed by resting-state fMRI. *Cereb Cortex*. 21:145–154.

Friston KJ, Williams S, Howard R, Frackowiak RS, Turner R. 1996. Movement-related effects in fMRI time-series. *Magn Reson Med*. 35:346–355.

Gao W, Alcauter S, Elton A, Hernandez-Castillo CR, Smith JK, Ramirez J, Lin W. 2015a. Functional network development during the first year: relative sequence and socioeconomic correlations. *Cereb Cortex*. 25:2919–2928.

Gao W, Alcauter S, Smith JK, Gilmore JH, Lin W. 2015b. Development of human brain cortical network architecture during infancy. *Brain Struct Funct*. 220:1173–1186.

Gao W, Elton A, Zhu H, Alcauter S, Smith JK, Gilmore JH, Lin W. 2014. Intersubject variability of and genetic effects on the brain's functional connectivity during infancy. *J Neurosci*. 34:11288–11296.

Gao W, Gilmore JH, Giovanello KS, Smith JK, Shen D, Zhu H, Lin W. 2011. Temporal and spatial evolution of brain network topology during the first two years of life. *PLoS One*. 6: e25278.

Gao W, Lin W, Grewen K, Gilmore JH. 2017. Functional connectivity of the infant human brain: plastic and modifiable. *Neuroscientist*. 23:169–184.

Gilmore JH, Knickmeyer RC, Gao W. 2018. Imaging structural and functional brain development in early childhood. *Nat Rev Neurosci*. 19:123–137.

Gong G, He Y, Evans AC. 2011. Brain connectivity: gender makes a difference. *Neuroscientist*. 17:575–591.

Gordon EM, Laumann TO, Gilmore AW, Newbold DJ, Greene DJ, Berg JJ, Ortega M, Hoyt-Drazen C, Gratton C, Sun H, et al. 2017. Precision functional mapping of individual human brains. *Neuron*. 95:791–807.e797.

Gozdas E, Holland SK, Altaye M. 2019. Developmental changes in functional brain networks from birth through adolescence. *Hum Brain Mapp*. 40:1434–1444.

Graham AM, Pfeifer JH, Fisher PA, Lin W, Gao W, Fair DA. 2015. The potential of infant fMRI research and the study of early life stress as a promising exemplar. *Dev Cogn Neurosci*. 12:12–39.

Gratton C, Laumann TO, Nielsen AN, Greene DJ, Gordon EM, Gilmore AW, Nelson SM, Coalson RS, Snyder AZ, Schlaggar BL, et al. 2018. Functional brain networks are dominated by stable group and individual factors, not cognitive or daily variation. *Neuron*. 98:439–452.e435.

Horien C, Noble S, Finn ES, Shen X, Scheinost D, Constable RT. 2018. Considering factors affecting the connectome-based identification process: comment on Waller et al. *Neuroimage*. 169:172–175.

Horien C, Shen X, Scheinost D, Constable RT. 2019. The individual functional connectome is unique and stable over months to years. *Neuroimage*. 189:676–687.

Hughes E, Cordero-Grande L, Murgasova M, Hutter J, Price A, Gomes ADS, Allsop J, Steinweg J, Tusor N, Wurie J, *et al*. 2017. The developing human connectome: announcing the first release of open access neonatal brain imaging. In. *The 23rd Annual Meeting of the Organization for Human Brain Mapping; Vancouver (Canada)*.

Jakab A, Schwartz E, Kasprian G, Gruber GM, Prayer D, Schöpf V, Langs G. 2014. Fetal functional imaging portrays heterogeneous development of emerging human brain networks. *Front Hum Neurosci*. 8:852.

Kaufmann T, Alnaes D, Doan NT, Brandt CL, Andreassen OA, Westlye LT. 2017. Delayed stabilization and individualization in connectome development are related to psychiatric disorders. *Nat Neurosci*. 20:513–515.

Kelly C, Biswal BB, Craddock RC, Castellanos FX, Milham MP. 2012. Characterizing variation in the functional connectome: promise and pitfalls. *Trends Cogn Sci*. 16:181–188.

Krzywinski M, Schein J, Birol I, Connors J, Gascoyne R, Horsman D, Jones SJ, Marra MA. 2009. Circos: an information aesthetic for comparative genomics. *Genome Res*. 19:1639–1645.

Laumann TO, Gordon EM, Adeyemo B, Snyder AZ, Joo SJ, Chen MY, Gilmore AW, McDermott KB, Nelson SM, Dosenbach NU, et al. 2015. Functional system and areal organization of a highly sampled individual human brain. *Neuron*. 87:657–670.

Liao X, Cao M, Xia M, He Y. 2017. Individual differences and time-varying features of modular brain architecture. *Neuroimage*. 152:94–107.

Liu J, Liao X, Xia M, He Y. 2018. Chronnectome fingerprinting: identifying individuals and predicting higher cognitive functions using dynamic brain connectivity patterns. *Hum Brain Mapp*. 39:902–915.

Mitra A, Snyder AZ, Tagliazucchi E, Laufs H, Elison J, Emerson RW, Shen MD, Wolff JJ, Botteron KN, Dager S, et al. 2017. Resting-state fMRI in sleeping infants more closely resembles adult sleep than adult wakefulness. *PLoS One*. 12:e0188122.

Mueller S, Wang D, Fox MD, Yeo BT, Sepulcre J, Sabuncu MR, Shafee R, Lu J, Liu H. 2013. Individual variability in functional connectivity architecture of the human brain. *Neuron*. 77:586–595.

Murphy K, Fox MD. 2017. Towards a consensus regarding global signal regression for resting state functional connectivity MRI. *Neuroimage*. 154:169–173.

Newman ME, Girvan M. 2004. Finding and evaluating community structure in networks. *Phys Rev E Stat Nonlin Soft Matter Phys*. 69:026113.

Noble S, Spann MN, Tokoglu F, Shen X, Constable RT, Scheinost D. 2017. Influences on the test-retest reliability of functional connectivity MRI and its relationship with behavioral utility. *Cereb Cortex*. 27:5415–5429.

Ouyang M, Kang H, Detre JA, Roberts TPL, Huang H. 2017. Short-range connections in the developmental connectome during typical and atypical brain maturation. *Neurosci Biobehav Rev*. 83:109–122.

Power JD, Barnes KA, Snyder AZ, Schlaggar BL, Petersen SE. 2012. Spurious but systematic correlations in functional connectivity MRI networks arise from subject motion. *Neuroimage*. 59:2142–2154.

Power JD, Barnes KA, Snyder AZ, Schlaggar BL, Petersen SE. 2013. Steps toward optimizing motion artifact removal in functional connectivity MRI; a reply to Carp. *Neuroimage*. 76:439–441.

Power JD, Cohen AL, Nelson SM, Wig GS, Barnes KA, Church JA, Vogel AC, Laumann TO, Miezin FM, Schlaggar BL, et al. 2011. Functional network organization of the human brain. *Neuron*. 72:665–678.

Power JD, Plitt M, Laumann TO, Martin A. 2017. Sources and implications of whole-brain fMRI signals in humans. *Neuroimage*. 146:609–625.

Power JD, Schlaggar BL, Petersen SE. 2015. Recent progress and outstanding issues in motion correction in resting state fMRI. *Neuroimage*. 105:536–551.

Rosenberg MD, Finn ES, Scheinost D, Papademetris X, Shen X, Constable RT, Chun MM. 2016. A neuromarker of sustained attention from whole-brain functional connectivity. *Nat Neurosci*. 19:165–171.

Rosvall M, Bergstrom CT. 2008. Maps of random walks on complex networks reveal community structure. *Proc Natl Acad Sci U S A*. 105:1118–1123.

Salimi-Khorshidi G, Douaud G, Beckmann CF, Glasser MF, Griffanti L, Smith SM. 2014. Automatic denoising of functional MRI data: combining independent component analysis and hierarchical fusion of classifiers. *Neuroimage*. 90:449–468.

Satterthwaite TD, Wolf DH, Loughead J, Ruparel K, Elliott MA, Hakonarson H, Gur RC, Gur RE. 2012. Impact of in-scanner head motion on multiple measures of functional connectivity: relevance for studies of neurodevelopment in youth. *Neuroimage*. 60:623–632.

Shi F, Salzwedel AP, Lin W, Gilmore JH, Gao W. 2018. Functional brain parcellations of the infant brain and the associated developmental trends. *Cereb Cortex*. 28:1358–1368.

Shi F, Yap PT, Wu G, Jia H, Gilmore JH, Lin W, Shen D. 2011. Infant brain atlases from neonates to 1- and 2-year-olds. *PLoS One*. 6:e18746.

Smyser CD, Inder TE, Shimony JS, Hill JE, Degnan AJ, Snyder AZ, Neil JJ. 2010. Longitudinal analysis of neural network development in preterm infants. *Cereb Cortex*. 20:2852–2862.

Stoecklein S, Hilgendorff A, Li M, Förster K, Flemmer AW, Galiè F, Wunderlich S, Wang D, Stein S, Ehrhardt H, et al. 2020. Variable functional connectivity architecture of the preterm human brain: impact of developmental cortical expansion and maturation. *Proc Natl Acad Sci U S A*. 117:1201–1206.

Thomason ME, Grove LE, Lozon TA Jr, Vila AM, Ye Y, Nye MJ, Manning JH, Pappas A, Hernandez-Andrade E, Yeo L, et al. 2015. Age-related increases in long-range connectivity in fetal functional neural connectivity networks in utero. *Dev Cogn Neurosci*. 11:96–104.

Tzourio-Mazoyer N, Landeau B, Papathanassiou D, Crivello F, Etard O, Delcroix N, Mazoyer B, Joliot M. 2002. Automated anatomical labeling of activations in SPM using a macroscopic anatomical parcellation of the MNI MRI single-subject brain. *Neuroimage*. 15:273–289.

Van Dijk KR, Hedden T, Venkataraman A, Evans KC, Lazar SW, Buckner RL. 2010. Intrinsic functional connectivity as a tool for human connectomics: theory, properties, and optimization. *J Neurophysiol*. 103:297–321.

Van Dijk KR, Sabuncu MR, Buckner RL. 2012. The influence of head motion on intrinsic functional connectivity MRI. *Neuroimage*. 59:431–438.

Vanderwal T, Eilbott J, Finn ES, Craddock RC, Turnbull A, Castellanos FX. 2017. Individual differences in functional connectivity during naturalistic viewing conditions. *Neuroimage*. 157:521–530.

Vértes PE, Bullmore ET. 2015. Annual research review: Growth connectomics–the organization and reorganization of brain networks during normal and abnormal development. *J Child Psychol Psychiatry*. 56:299–320.

Vinh NX, Epps J, Bailey J. 2010. Information theoretic measures for clusterings comparison: variants, properties, normalization and correction for chance. *J Mach Learn Res*. 11:2837–2854.

Wang J, Wang X, Xia M, Liao X, Evans A, He Y. 2015. GRETNA: a graph theoretical network analysis toolbox for imaging connectomics. *Front Hum Neurosci*. 9:386.

Weissenbacher A, Kasess C, Gerstl F, Lanzenberger R, Moser E, Windischberger C. 2009. Correlations and anticorrelations in resting-state functional connectivity MRI: a quantitative comparison of preprocessing strategies. *Neuroimage*. 47:1408–1416.

Whitlow CT, Casanova R, Maldjian JA. 2011. Effect of resting-state functional MR imaging duration on stability of graph theory metrics of brain network connectivity. *Radiology*. 259:516–524.

Xia M, Wang J, He Y. 2013. BrainNet Viewer: a network visualization tool for human brain connectomics. *PLoS One*. 8:e68910.

Xu Y, Cao M, Liao X, Xia M, Wang X, Jeon T, Ouyang M, Chalak L, Rollins N, Huang H, et al. 2019. Development and emergence of individual variability in the functional connectivity architecture of the preterm human brain. *Cereb Cortex*. 29:4208–4222.

Yan CG, Craddock RC, Zuo XN, Zang YF, Milham MP. 2013. Standardizing the intrinsic brain: towards robust measurement of inter-individual variation in 1000 functional connectomes. *Neuroimage*. 80:246–262.

Zhang H, Stanley N, Mucha PJ, Yin W, Lin W, Shen D. 2018. Multilayer large-scale functional connectome reveals infant brain developmental patterns. In: Frangi A, Schnabel J, Davatzikos C, Alberola-López C, Fichtinger G, editors. Medical Image Computing and Computer Assisted Intervention - MICCAI 2018. Lecture Notes in Computer Science, vol 11072. Granada (Spain): Springer, 136–144.

Zhao T, Xu Y, He Y. 2019. Graph theoretical modeling of baby brain networks. *Neuroimage*. 185:711–727.